



HAL
open science

Impact of orbiting satellites on star formation rate evolution and metallicity variations in Milky Way-like discs

Bhargav Annem, Sergey Khoperskov

► **To cite this version:**

Bhargav Annem, Sergey Khoperskov. Impact of orbiting satellites on star formation rate evolution and metallicity variations in Milky Way-like discs. *Monthly Notices of the Royal Astronomical Society*, 2023, 527 (2), pp.2426-2436. 10.1093/mnras/stad3244 . hal-03850976

HAL Id: hal-03850976



<https://hal.science/hal-03850976>

Submitted on 22 Apr 2024

HAL is a multi-disciplinary open access archive for the deposit and dissemination of scientific research documents, whether they are published or not. The documents may come from teaching and research institutions in France or abroad, or from public or private research centers.

L'archive ouverte pluridisciplinaire **HAL**, est destinée au dépôt et à la diffusion de documents scientifiques de niveau recherche, publiés ou non, émanant des établissements d'enseignement et de recherche français ou étrangers, des laboratoires publics ou privés.

Impact of orbiting satellites on star formation rate evolution and metallicity variations in Milky Way-like discs

Bhargav Annem¹   and Sergey Khoperskov^{2,3}

¹California Institute of Technology, 1200 E California Blvd, Pasadena, CA 91125, USA

²Leibniz Institut für Astrophysik Potsdam (AIP), An der Sternwarte 16, D-14482 Potsdam, Germany

³GEPI, Observatoire de Paris, Université PSL, CNRS, 5 Place Jules Janssen, F-92190 Meudon, France

Accepted 2023 October 18. Received 2023 October 18; in original form 2022 November 8

ABSTRACT

At least one major merger is currently taking place in the Milky Way (MW). The Sagittarius (Sgr) dwarf galaxy is being tidally destroyed while orbiting around the MW, whose close passages perturb the disc externally. In this work, using hydrodynamical simulations, we investigate how massive dwarf galaxies on quasi-polar Sgr-like orbits impact the star formation (SF) inside the MW-like discs. First, we confirm that interactions with orbiting satellites enhance the SF rate in the host. However, prominent SF bursts are detected during the very close passages (<20 kpc) of massive ($2 \times 10^{10} M_{\odot}$) gas-poor satellites. For gas-rich satellites, while we observe substantial enhancement of the SF, we do not detect prominent peaks in the SF history of the host. This can be explained by the steady gas accretion from the satellite smoothening short-term variations in the SF. The impact of the satellite perturbations, especially its first encounters, is seen mainly in the outer (>10 kpc) disc. We also found that the close passages of satellites cause the formation of low-metallicity stars in the host, and the effect is the most prominent for gas infall from the satellites resulting in the dilution of the mean stellar metallicity. Our simulations are in favour of causality between the recent passages of the Sgr and the bursts of the SF in the solar neighbourhood (≈ 1 and ≈ 2 Gyr ago); however, to reproduce the SF burst at its first infall (≈ 6 Gyr), we require a very close passage (<20 kpc) with subsequent substantial mass-loss of the Sgr precursor.

Key words: galaxies: evolution – galaxies: formation – galaxies: star formation.

1 INTRODUCTION

The Milky Way (MW) is believed to be a typical disc galaxy with a central bar and boxy/peanut bulge in the centre (Dwek et al. 1995; Wegg & Gerhard 2013; Ness & Lang 2016) and extended, likely flocculent, multi-arm spiral structure (Vallée 2005; Reid et al. 2009; Bland-Hawthorn & Gerhard 2016). The outer disc of the MW is warped relative to the disc mid-plane inside the solar circle (Kerr 1957; Drimmel & Spergel 2001; Poggio et al. 2018). The presence of the warp is believed to be a manifestation of the interaction with a massive galaxy companion (see e.g. Ibata & Razoumov 1998; Bailin 2003; D’Onghia et al. 2016; Laporte et al. 2018a, b). Different models have been proposed to identify the mechanism of its formation, and it is generally believed that the Sagittarius (Sgr) dwarf galaxy (Ibata, Gilmore & Irwin 1994, 1995) could have been the most prominent external perturber of the MW disc (Bailin 2003; Michel-Dansac et al. 2011; Purcell et al. 2011; Gómez et al. 2013; Schönrich & Dehnen 2018). Although some alternative ideas have not been ruled out (Darling & Widrow 2019; Khoperskov et al. 2019), it is supposed that the recent passages of the Sgr dwarf galaxy are responsible for the emergence of the phase-space snail in the solar neighbourhood

(SND; Antoja et al. 2018; Bland-Hawthorn et al. 2019; Laporte et al. 2019, but an extensive discussion of lacunae in this theory can be found in Bennett & Bovy 2021; Bennett, Bovy & Hunt 2022).

Recently, it was also proposed that recurrent perturbations of the MW disc caused by the Sgr dwarf galaxy can temporally enhance the star formation (SF) in the disc (Ruiz-Lara et al. 2020). Using the *Gaia* Data Release 2 (DR2) data (Gaia Collaboration 2018), Ruiz-Lara et al. (2020) recovered the SF history (SFH) in a local volume around the SND. A striking feature of the recovered SFH (or age distribution) is multiple distinct bursts (1, 2, and ≈ 6 Gyr ago) of the SF (see also Cignoni et al. 2006, who found the SF bursts in the MW ≈ 2 and 4–6 Gyr ago), which correlate with the predicted pericentric passages of the Sgr dwarf galaxy (Law & Majewski 2010; Purcell et al. 2011; de la Vega et al. 2015; Laporte et al. 2018b). It is important to note that there are some other models that expect the pericentric passages to happen at slightly different times (see e.g. Dierickx & Loeb 2017; Gibbons, Belokurov & Evans 2017; Tepper-García & Bland-Hawthorn 2018; Dillamore et al. 2022). The discrepancies between different models of the Sgr orbital motion naturally arise from the uncertainties in the mass-loss over time (see e.g. Jiang & Binney 2000; Gibbons et al. 2017; Bland-Hawthorn & Tepper-García 2021), thus affecting the dynamical friction strength and expected perturbations of the MW potential (D’Souza & Bell 2022). This affects the Sgr stream used to constrain the orbit of the Sgr precursor (Gómez et al. 2015; Vasiliev,

* E-mail: bannem@caltech.edu

Belokurov & Erkal 2021). Another approach to date the pericentric passages of dwarfs is based on the timing of SF episodes inside these satellite galaxies (see e.g. Sohn et al. 2007; Pasetto et al. 2011; Rusakov et al. 2021). Indeed, grasping the underlying physics driving increased SF due to interactions holds profound significance, as it offers means to extract orbital parameters of interacting systems (the Small Magellanic Cloud–Large Magellanic Cloud system; Massana et al. 2022) and it enables deeper insights into past events in the evolution of dwarf galaxies (e.g. Leo I; Ruiz-Lara et al. 2021). In the case of the Sgr dwarf and its stream, different authors found several episodes of SF: 0.5, 5, and 11 Gyr ago (Layden & Sarajedini 2000); 5–7, 11, and 13 Gyr ago (de Boer, Belokurov & Koposov 2015); and 2.3, 4, and 6 Gyr ago (Siegel et al. 2007). To summarize, several recent works report that both MW and Sgr precursor have experienced several bursts of SF in the last ≈ 6 Gyr and some of these bursts could have happened at the moments of pericentric passages of the Sgr.

Generally speaking, different models suggest that interactions and mergers with sufficiently massive dwarf galaxies, under certain conditions, may enhance the SF in the main galaxy (Barnes & Hernquist 1991; Jog & Solomon 1992; Mihos & Hernquist 1994; Springel, Di Matteo & Hernquist 2005; Cox et al. 2008; Renaud et al. 2014; Moreno et al. 2015; Sparre & Springel 2016; Renaud, Segovia Otero & Agertz 2022). This effect depends on the parameters of interaction such as the perturber’s orbit, relative mass, and relative gas fraction (Di Matteo et al. 2007, 2008; Hopkins et al. 2013a; Moreno et al. 2015; Pettitt et al. 2017). For instance, Di Cintio et al. (2021) found a reasonable correlation between the peaks of SF and pericentric passages of massive dwarfs in the CLUES (Constrained Local Universe Simulations). A similar effect was demonstrated using the HESTIA (High-resolution Environmental Simulations of The Immediate Area) simulations of the Local Group (Khoperskov et al. 2023a), where it was suggested that not all close passages or fly-bys of dwarf galaxies enhance the SF (see also Di Matteo et al. 2007; Renaud et al. 2009, 2014). Despite the mounting growth of arguments in favour of Sgr-driven bursts of SF in the MW, it is inherently difficult to disentangle the impact of multiple perturbers moving on different orbits from internal processes (bar formation and evolution, and spiral arm formation) in cosmological models.

In this work, we aim to investigate the evolution of the SF rate (SFR) in controlled simulations of interaction between an MW-type disc galaxy and a massive dwarf galaxy on a nearly polar orbit. Although our work is inspired by the recent results suggesting a possible impact of the pericentric passages of the Sgr dwarf galaxy on the SF activity in the MW, we do not aim to reproduce the exact parameters of the Sgr dwarf galaxy and the observed configuration of its tidal streams. The paper is organized as follows. In Section 2, we describe the initial conditions of our models and the simulation set-up. In Sections 3.1–3.4, we analyse the SFH features of the MW-like galaxies depending on the gas content, masses, and pericentric distances of orbiting satellites. In Section 3.5, we present the metallicity behaviour of stars in the host galaxy under influence of massive satellite. In Section 4, we discuss the MW–Sgr interaction in the context of our simulations. Finally, in Section 5, we summarize our main findings.

2 MODELS

2.1 Initial conditions for the host and dwarf galaxies

Initial conditions for the host and satellite galaxy were generated using the AGAMA software (Vasiliev 2019). In all of our simulations,

Table 1. Parameters of models. The model ISO is an isolated MW-type galaxy simulation, while others include the dynamics of satellite galaxy of different mass and different gas amount. Initial coordinates of satellite galaxies are $[125, 0, 0]$ and $v_y = 0 \text{ km s}^{-1}$, while the centre of the host galaxy is located at $[0, 0, 0]$. The parameters of the host galaxy are the same across the models and described in Section 2.1.

Model name	Satellite DM mass ($10^{10} M_{\odot}$)	Satellite stellar mass ($10^{10} M_{\odot}$)	Satellite gas mass ($10^{10} M_{\odot}$)	v_x (km s^{-1})	v_z (km s^{-1})
ISO	–	–	–	–	–
M1noG	5	1	–	–10	120
M2noG	5	1	–	–30	80
S1noG	1.6	0.4	–	–40	50
S2noG	1.6	0.4	–	0	90
M1	5	0.5	0.5	–10	120
M2	5	0.5	0.5	–30	80
S1	1.6	0.2	0.2	–40	50
S2	1.6	0.2	0.2	0	90

the initial set-up for the host galaxy is identical and has three components (dark matter, pre-existing stars, and gas), and has the following initial settings. The initial stellar disc is represented by a Miyamoto–Nagai density profile (Miyamoto & Nagai 1975) with a characteristic scale length of 4 kpc, vertical thicknesses of 0.3 kpc, and a mass of $6 \times 10^{10} M_{\odot}$. The simulation includes a live dark matter halo (2×10^6 particles) whose density distribution follows a Plummer sphere (Plummer 1911) with a total mass of $9.2 \times 10^{11} M_{\odot}$ and a scale radius of 21 kpc. The gas component initially features 10^6 particles with a mass of $1 \times 10^4 M_{\odot}$, which can be partially converted into newly formed stars. The gas is distributed in a thin disc component following a Miyamoto–Nagai density distribution with a scale length of 5 kpc. This choice of parameters leads to a galaxy mass model with a circular velocity of $\approx 230 \text{ km s}^{-1}$.

We study the impact of both high-mass and low-mass satellites with a total mass of 2×10^{10} and $6 \times 10^{10} M_{\odot}$, respectively. The dark matter (DM) component of the satellite is represented by 2.5×10^5 particles redistributed following a Navarro–Frenk–White (NFW) model with a scale length of 10 kpc. Stars (10^5 particles) are initially distributed using a Plummer model with a scale length of 4 kpc. The gas is considered as a Miyamoto–Nagai disc with a characteristic scale length of 2 kpc with a mass of gas particles of $1 \times 10^4 M_{\odot}$. The masses of the DM, stellar, and gas components are shown in Table 1. In the table, we also provide the initial velocity of the satellite, which is located in the host galaxy plane at $x = 125$ kpc from its centre (similar to Dierickx & Loeb 2017; Tepper-García & Bland-Hawthorn 2018). In this work, we study the impact of the satellite on a polar orbit, which is similar to the orbit of the Sgr dwarf galaxy (e.g. Gómez et al. 2015; Gibbons et al. 2017). In total, we run a few dozen different models where we varied the initial velocity component of the satellite in a wide range, but in this paper we only present eight models, which provide us with an orbit that is quantitatively similar to the Sgr and, especially in the case of massive satellites, do not rapidly merge. The full set of models considered here includes models with gas in a satellite where we can capture the effects of the gas accretion from the satellite together with gasless models (inside the satellite) where we can study the purely kinematic impact on the host galaxy SF. The SFHs of the host galaxies are also compared to those of the isolated host galaxy evolution (model ISO).

In order to investigate the impact of the satellite passages on the metallicity distribution in the host galaxies, we initialize the radial metallicity profile of the interstellar medium (ISM) in both host and

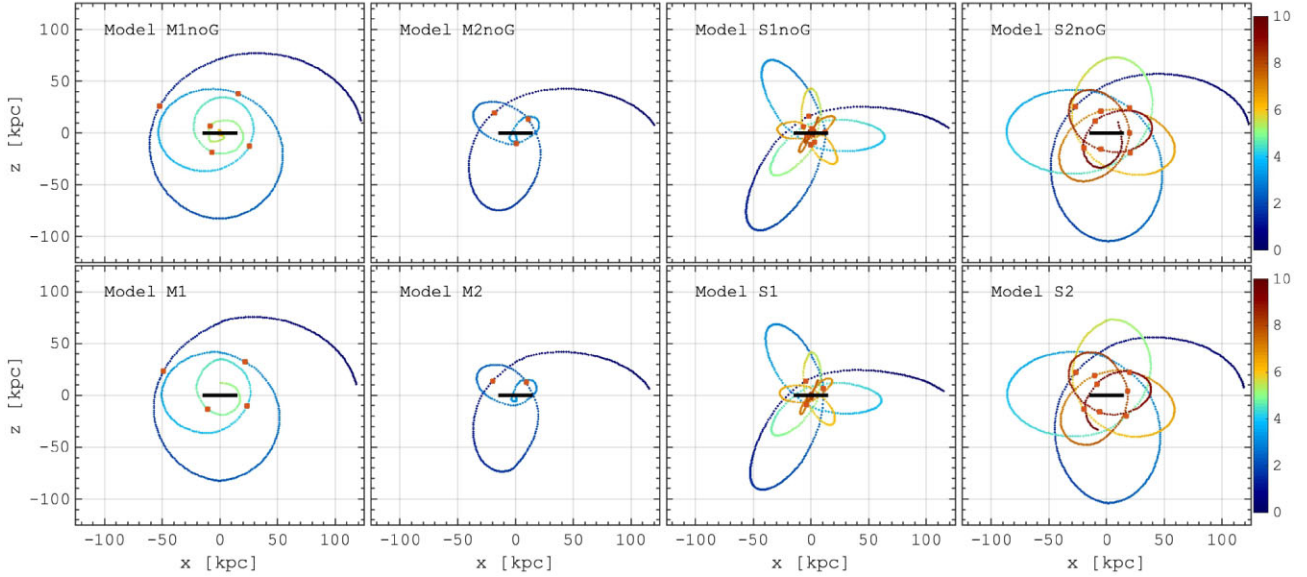


Figure 1. Orbits of satellites in different models. The top row corresponds to the models with a gasless satellite, while the bottom shows the gas-rich satellites. The XZ-projections of the orbits are shown where the disc of the host galaxy is located in XY-plane, highlighted by the black line, representing a 15 kpc radial scale. The orbits of the satellites are colour-coded by the integration time in Gyr as shown in the colour bars. The red squares highlight moments of pericentric passages of the orbiting satellites.

satellite galaxies. Since newborn stars inherit their abundances from the gas component, radial redistribution and accretion of gas from the satellite would affect the metallicity distribution of the host. Since we do not aim to fit any particular data set in this work, we adopted the negative metallicity gradients of -0.13 and -0.05 dex kpc^{-1} with the central value of 0.1 and -0.5 dex for the host and satellite galaxies, respectively. Nevertheless, the metallicity gradient for the host galaxy chosen is in agreement with some recent estimations for the MW disc ≈ 10 Gyr ago (Lu et al. 2022; Ratcliffe et al. 2023). The adopted metallicity gradient value for the dwarf galaxy is typical for nearby dwarf galaxies (see e.g. Taibi et al. 2022).

In this work, we run a series of simulations of galaxy mergers that used the hybrid N -body/hydro code GIZMO (Hopkins 2015, 2017). We invoked the meshless finite mass hydrodynamical solver and an adaptive gravitational softening for the gas. The Springel & Hernquist (2003) multiphase interstellar medium (ISM) algorithm has been used, and the feedback includes the Type I and Type II supernova. Following Hopkins, Narayanan & Murray (2013b) and Hopkins (2017), the SF was allowed only in virialized regions.

2.2 Orbits of satellites

In Fig. 1, we present the XZ-projections of the satellites' orbits where the host galaxy is placed in the XY plane. Remember that in this work, we study the interactions of the MW-type galaxies with satellites on a polar orbit. The top row corresponds to the models without gas in the satellites, and the bottom row shows the orbits of gas-rich satellites. Note that the orbits in these two cases are nearly identical because the total mass of the satellites is the same in both set-ups. Thus, they experienced a very similar evolution due to a comparable impact of dynamical friction dragging satellite galaxies towards the centre of the host. The first two columns show the orbits of massive satellites, while low-mass satellites are shown in the two rightmost columns (see Table 1 for the model parameters). In the case of massive satellites, the merger is completed on a relatively short time-scale, and we do not study the evolution of these models

after that ≈ 3 – 5 Gyr. In this case, we have access to 3–4 pericentric passages, marked with red squares in Fig. 1. Meanwhile, the low-mass satellites experience a long-term evolution, slowly swinging towards the centre of the host for about 8–10 Gyr. In these models, we detected more than eight pericentric passages. In all of the models, the pericentric distances decrease with time, thus making it possible to study the impact of the satellites on the SF in the host galaxy at different distances in just a few models. Also, note that although we do not aim to reproduce the motion of the Sgr dwarf galaxy, the orbits of our satellite galaxies are quite similar to some previous models of the Sgr orbit (see e.g. Purcell et al. 2011; Dierickx & Loeb 2017; Tepper-García & Bland-Hawthorn 2018, for reference), thus suggesting that our conclusions can be extrapolated on the impact of the Sgr on the SF in the MW.

3 RESULTS

In this section, we investigate the connection between the SF evolution of the MW-like hosts and recurrent perturbations by satellite galaxies orbiting around.

3.1 Models with no gas inside satellite galaxies

First, we discuss the evolution of models with no gas inside satellite galaxies (models M1noG, M2noG, S1noG, and S2noG). In Fig. 2, we show the orbital decay of the satellite galaxies in different models together with the SFHs of the host galaxies. The SF in the host considers only stars that are being formed in the disc within $R_{\text{gal}} = 25$ kpc and not beyond 2 kpc from the mid-plane. Also, to ensure that we do not include any stars formed in the satellite galaxies inside this region, we count only stars if their absolute value of the initial vertical velocity is below 50 km s^{-1} . However, the latest criterion starts to be important at the very last episodes of the merger. In each panel, the SFR of the host galaxy (blue line) is compared to the one in the isolated galaxy simulation (grey area), where, in order to put all the panels on the same scale, we normalize both (interacting

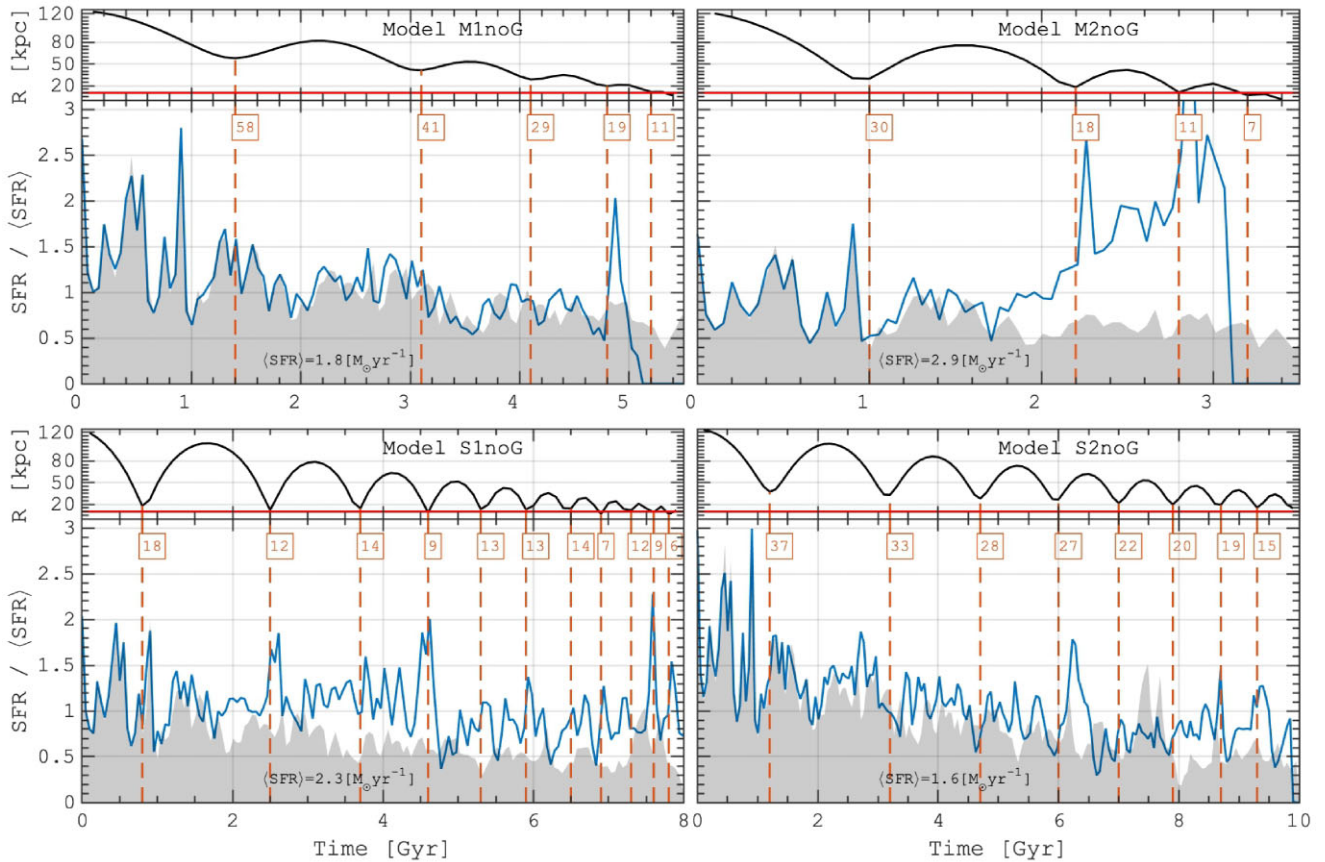


Figure 2. Orbital decay of satellites and SFHs of the host galaxies. The top sub-panels show the orbital decay of satellite galaxies, while the bottom ones show the evolution of the SFH in the host galaxies. The SFHs are shown by the blue lines and compared to the SFH in the isolated host simulation, shown by the grey-filled area. For a better comparison between different models, in each panel, both SFHs are normalized by the mean SFR in the interacting case ($\langle SFR \rangle$), marked in each panel. The red vertical lines highlight moments of pericentric passages where the pericentric distance (in kpc) is shown in the corresponding red boxes.

and isolated) SFHs by the mean SFR ($\langle SFR \rangle$, see the values in each panel) in the interacting simulation. For each SFH plot, we show the red vertical lines that correspond to the pericentric passages of the dwarf galaxies, where the pericentric distances are marked accordingly.

We start our analysis from the massive dwarf simulations ($\approx 6 \times 10^{10} M_{\odot}$) shown in the top row of Fig. 2. In model M1noG, we can see that the SFH is nearly identical to the isolated one until the latest pericentric passage (19 kpc) at ≈ 4.8 Gyr. In this case, the SFR rapidly increased by a factor of ≈ 2 compared to the isolated simulation. This suggests that even a very massive dwarf galaxy does not significantly affect the SFR in the host galaxy while it is orbiting at distances > 20 kpc. The same result is seen in model M2noG, where the first passage, at 30 kpc, has no impact on the SFR of the host. However, the next pericentre (≈ 18 kpc) corresponds to a prominent peak of the SF. Note, however, that in this model, the SFR starts to increase gradually sometime before the second pericentre. The next sharp peak in the SFH also correlates with the next, even closer pericentric passage (≈ 11 kpc). Even with no extra gas infall from the satellite, the overall SFR is much higher compared to the isolated simulation, which suggests that only the gas of the host is involved in the SF. Therefore, the increase of the SFR is due to the contraction of the gas caused by rapidly strengthened tidal forces (Renaud et al. 2009, 2014, 2022) during the close passages of the satellite galaxy.

In the lower mass satellite simulations ($\approx 1.2 \times 10^{10} M_{\odot}$, see bottom row of Fig. 2), we can see a similar behaviour of the SF as above. For instance, in model S1noG, we see many peaks of the SFR corresponding to a number of the pericentric passages, except for the first one at 18 kpc. This simply shows that lower mass systems need to come close to the host compared to the higher mass satellites in order to trigger the SF burst. This is also evident in model S2noG where most of the pericentric distances are quite far from the centre of the host, and only the latest two passages (19 and 15 kpc) correlate with the prominent short time-scale increase of the SFR.

To summarize, in the case of pure tidal interaction between gasless satellites and massive MW-type disc galaxies, the SF increases in the hosts if the pericentric distance is smaller than ≈ 20 kpc. At larger distances, we do not detect any significant effects, even in the case of massive ($\approx 6 \times 10^{10} M_{\odot}$) perturber.

3.2 Models with gas-rich satellite galaxies

Next, we discuss the behaviour of the SFR in the simulations, which include a substantial amount of gas inside the satellite galaxies. In such models, we can follow the impact of the infall of gas stripped from the satellite galaxies and thus compare its contribution to the SFR of the host undergoing the purely kinetic perturbations

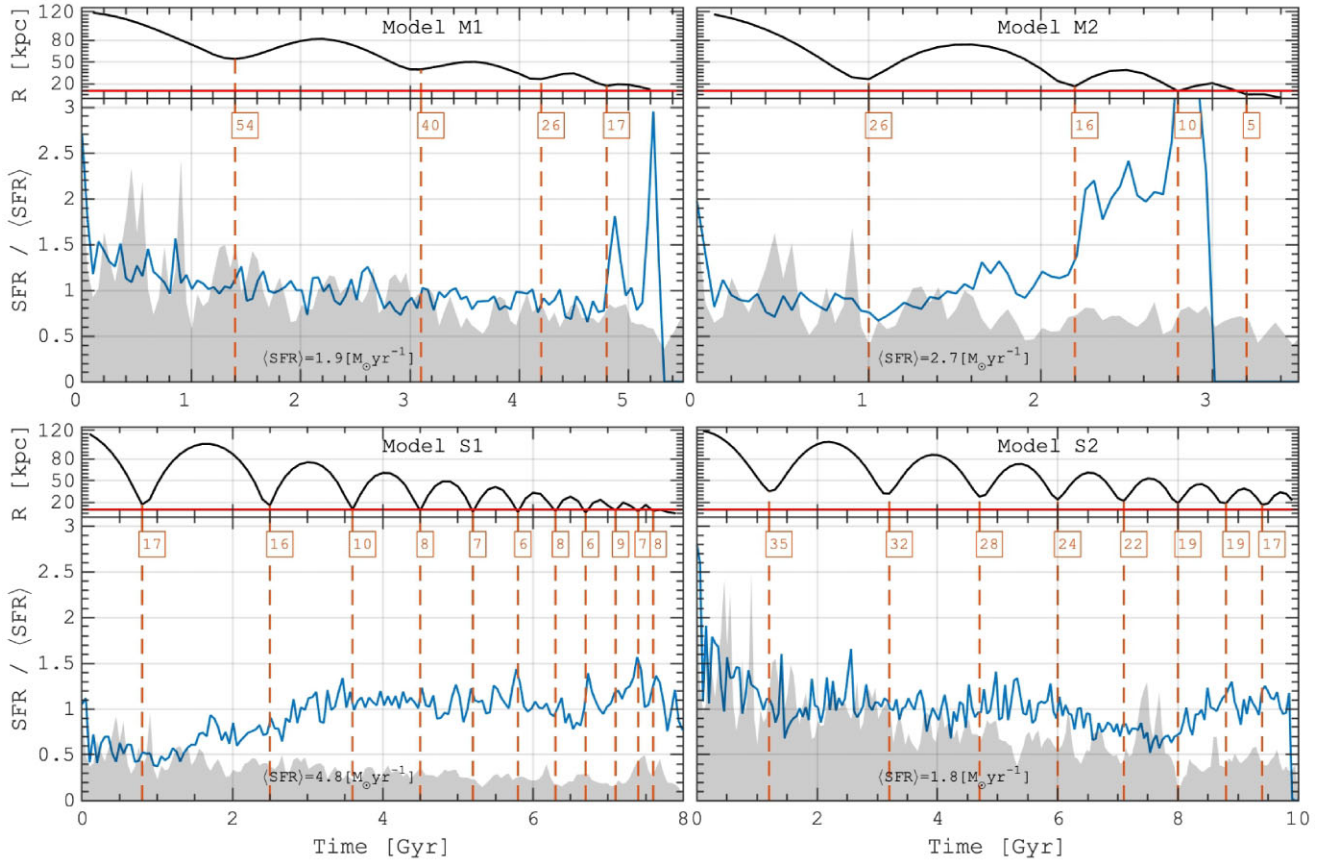


Figure 3. Same as in Fig. 2, but for gas-rich satellites. Note that the orbits of gas-rich satellites are identical to the gasless satellite simulations.

in gasless simulations as discussed above. Remember that in this set of simulations, we use the same mass models of dwarf galaxies resulting in very similar orbits and pericentric distances over time (see Fig. 1). Fig. 3 shows the orbital decay and SFH of the hosts compared to the isolated galaxy simulation. We notice that across all of the models with gas-rich satellites, the SFR is on average higher and the SFHs are significantly smoother when compared to the gasless satellite models and the isolated simulation. This is likely the result of the immediate interactions between the gas components of the host and satellite galaxies even at very early phases of evolution when the gas of the satellite is being stretched along the direction of the tidal forces (see also Tepper-García & Bland-Hawthorn 2018). Furthermore, the satellite gas being stripped along the orbit is constantly infalling on to the host. This results in a negligible effect of close passages on the SFR, which is seen in Fig. 3. In particular, although the SF is much higher on average, we do not detect any prominent bursts in model S1, which is the analogue of model S1nOG, where we observed multiple SF bursts. In gas-rich satellite simulations, local peaks of the SF are being observed only in the case of massive satellites (models M1 and M2) at the very last stages of the merger when the satellite crosses the disc of the host.

To summarize, in the case of gas-rich satellite interactions, we observe a higher mean SFR compared to gasless satellite simulations. However, the pericentric passages do not cause any prominent bursts of SF in the host galaxies. These results are in agreement with Renaud et al. (2021) who found that the infall of gas on to the galaxy, at the

early stages of the merger, is smooth, does not fuel the star-forming regions, and does not result in a rapid increase of the SF.

3.3 SF enhancement due to interactions

We showed that the mean SFR is higher in models with orbiting satellites compared to the isolated galaxy and it is higher even more if there is gas accretion from the satellites. However, which regions of the host galaxies are affected the most by the perturbations? In Fig. 4, we demonstrate the degree to which SF is enhanced in a given interacting model compared to the isolated galaxy simulation at different radii over time. The maps in the figure are colour-coded with the following parameters:

$$\delta(R_{\text{gal}}, t) = (\Sigma_{\text{int}}(R, t) - \Sigma_{\text{iso}}(R, t)) / (\Sigma_{\text{int}}(R, t) + \Sigma_{\text{iso}}(R, t)), \quad (1)$$

where Σ_{int} and Σ_{iso} are the SF surface density in interacting and isolated simulations, respectively. The parameter $\delta(R_{\text{gal}}, t)$ shows the degree to which the SFR in a pair of models is different. If it is negative, then the SFR is higher in the isolated galaxy; if it is close to zero, then the SFRs are comparable; and once it is close to 1, then the SFR in the isolated galaxy is negligible compared to the isolated galaxy model. The blue vertical lines highlight the pericentric passages of satellites if they are within 19 kpc. Otherwise, the arrows and numbers in blue boxes show the time and pericentric distance, respectively.

Fig. 4 clearly demonstrates that in our models, the SF is enhanced mostly in the outer regions of the host galaxy with a small variance

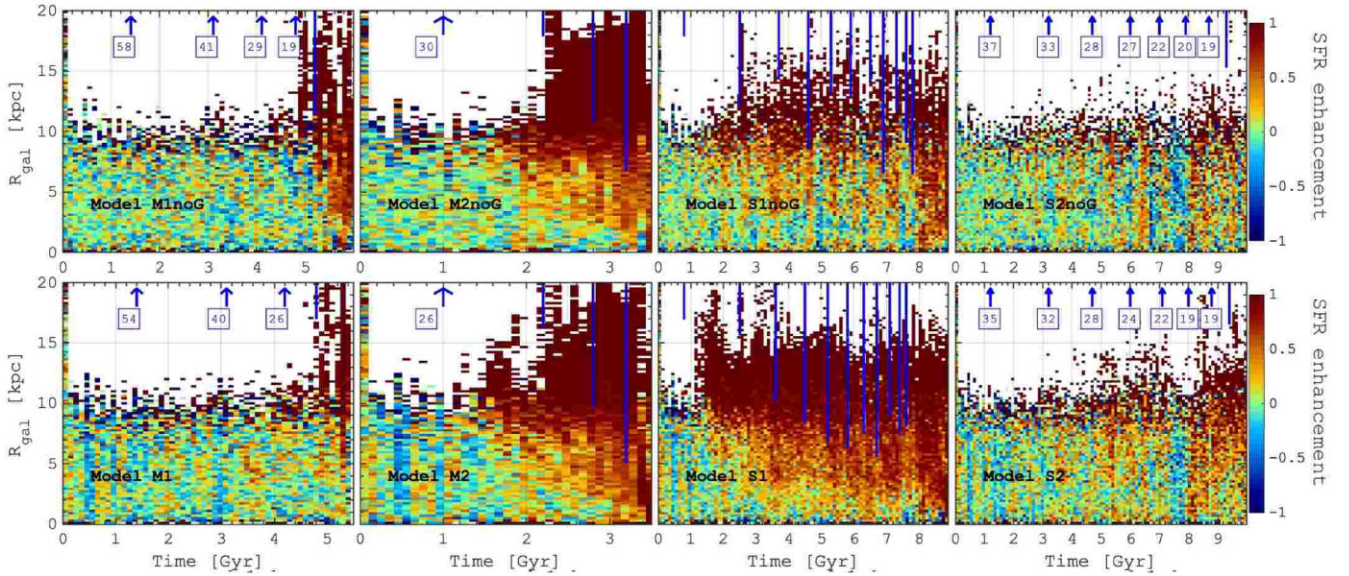


Figure 4. Relative enhancement of the SF in interacting models compared to the isolated one. The maps are colour-coded with following parameter $\delta(R_{\text{gal}}, t) = (\Sigma_{\text{int}} - \Sigma_{\text{int}})/(\Sigma_{\text{int}} + \Sigma_{\text{iso}})$ showing how much the SFR in the host galaxy is compared to the isolated model. The blue vertical lines highlight the moments of pericentric passages if the values are below 19 kpc; otherwise, the pericentres are marked by the arrows with the pericentric distance in kpc. Note that the vertical axis shows the galactocentric distance R_{gal} in cylindrical coordinates, while the pericentres correspond to a 3D distance to the host centre.

in the innermost region compared to the isolated simulation. In addition, all our models suggest that the SF starts to increase at ≈ 10 kpc once the satellites are sufficiently close to the host. Subsequently, the region of enhanced SF propagates slowly towards inner regions. However, even in models with strong impact (models M2noG, S1noG, M2, and S1), the inner regions show larger SF only several Gyr after the first close passage of the satellite. In these models, we also observe some SF out to 20 kpc, which is not the case in the isolated simulations with a weak perturbation from satellites.

The effect on the SF of the host we detected is strikingly similar to the kinematic response of the disc reported by Gómez et al. (2013), where the MW disc hosts prominent vertical density features at $R_{\text{gal}} > 8$ kpc (see their fig. 6). Carr et al. (2022) also showed the impact of a massive satellite in the outer disc, where the radial migration strength increases with radius and the guiding radius increases by more than 1 kpc explicitly where $R_{\text{gal}} > 8$ kpc (see their fig. 9).

In Fig. 5, we depict the proportional increase in gas surface density and SFR within the host galaxy plane, specifically focusing on simulation M2noG. This simulation is distinguished by the occurrence of two pericentric passages by a massive satellite before merging with the host. The upper panel illustrates the decay of the orbital trajectory, while the lower panels portray the instances immediately preceding, during, and immediately following each pericentric passage. The black crosses show the XY-position of the satellite galaxy at the corresponding times.

The enhancement, calculated as previously illustrated in Fig. 4, is referenced relative to the isolated simulation by using snapshots taken at equivalent time points. The depicted figure highlights that during the initial passage, there is a commencement of perturbation in gas density, primarily observable in the outer regions. This results in a marginal increase of the SFR, evident at distances greater than 10 kpc. A more recent and closer passage gives rise to prominent azimuthal variations in the parameters. Notably, the gas

distribution exhibits pronounced tidal structures, concomitant with a corresponding increase in the SFR. However, caution is exercised in establishing a direct link between the disc region impacted by a satellite and the heightened SFR, owing to the fact that interactions induce tidal structures, which tend to wind up rapidly (Dobbs et al. 2010; Pettitt, Tasker & Wadsley 2016), thus averaging out their impact along the azimuth. Consequently, even if the interaction with the Sgr triggers localized enhancement of the SFR within the MW, particularly within a specific quadrant, the rapid evolution and subsequent dissipation of tidal structures render such effects undetectable.

3.4 Star formation enhancement as a function of pericentric distance

In order to quantify the SF enhancement for each pericentric passage, we calculate the integrated SFR (ISFR), which is the total mass of stars formed over 0.5 Gyr after a given pericentric passage (see also Di Matteo et al. 2007):

$$\text{ISFR} = \int_{\tau}^{\tau+0.5 \text{ Gyr}} \text{SFR}(t) dt, \quad (2)$$

where $\text{SFR}(t)$ is the SFR, and τ is the time of pericentric passage of a satellite galaxy. We have chosen a time period of 0.5 Gyr to capture a pure effect of the interaction and avoid a possible overlap between two subsequent pericentric passages. In Fig. 6, different models are shown by different markers and colours. On the left, for each pericentric passage, the ISFR is normalized by the ISFR in the isolated simulation calculated over the same period of time, and it is shown as a function of the pericentric distance. The figure illustrates the previously described behaviour of the SFR in all of our simulations. In particular, we do not detect any systematic increase of the SF until 30 kpc; at closer passages (20–30 kpc), the SF intensity starts to increase, but it is still not larger by a factor of 2, relative to the isolated model. Only once the satellite galaxies

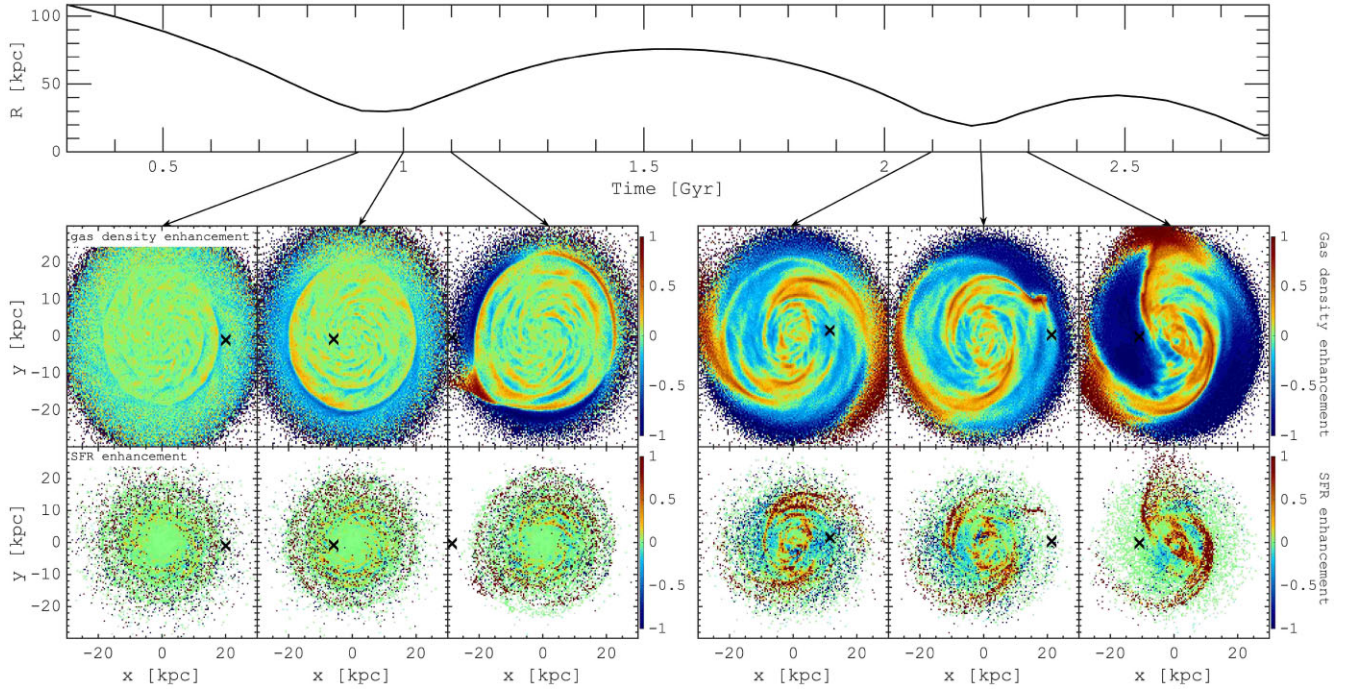


Figure 5. Relative gas density and SF enhancement in interacting models compared to the isolated one. *Top panel* shows the orbit of the satellite galaxy in model M2noG with two pericentric passages before coalescence. In *bottom panel*, the maps are colour-coded as in Fig. 4, showing how the gas density or SFR in the host galaxy is compared to the isolated model at the same times. The snapshots are chosen just before, during, and after a given pericentric passage.

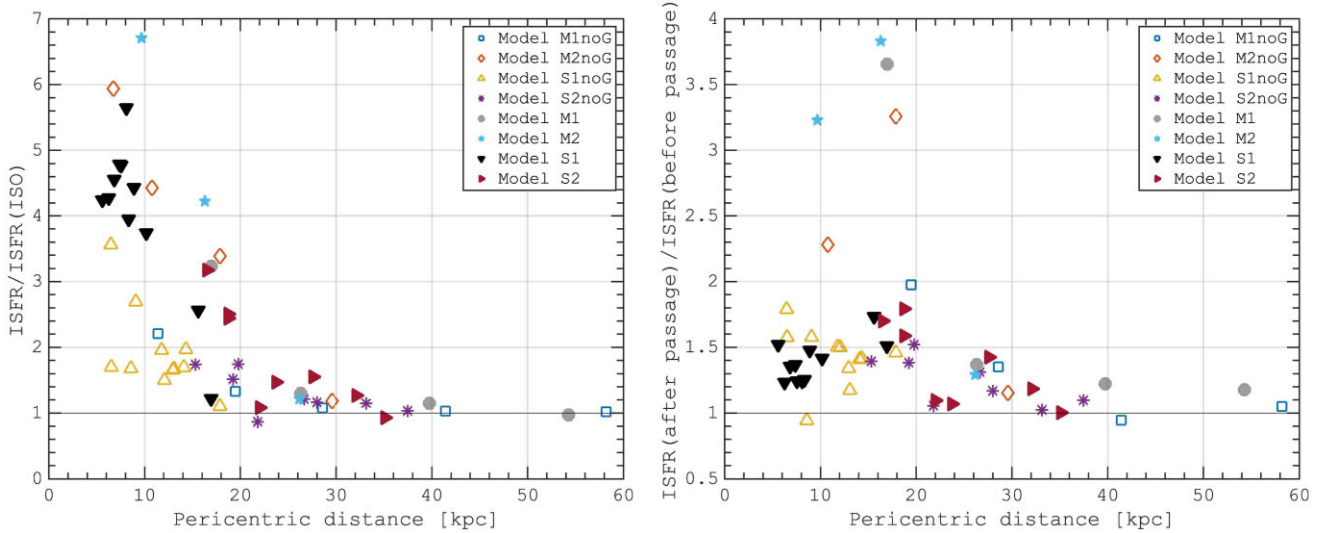


Figure 6. SFR enhancement as a function of pericentric distance. *In left:* the enhancement of the SF is calculated as a ratio between the ISFR (see equation 2) in interacting and isolated simulations. In both isolated and interacting simulations, the ISFRs are calculated over 0.5 Gyr after the corresponding pericentric passage. Our simulations show a lack of enhancement of the SF unless the satellites pass closer than ≈ 20 kpc in the case of $\leq 6 \times 10^{10} M_{\odot}$ satellite. *In right:* the enhancement of the SF is calculated in interacting simulations only as a ratio between the ISFR before and after the pericentric passage of the satellite galaxy.

pass within 20 kpc, the SF is enhanced by a factor of 2–4. For even closer pericentres, the SF enhancement is even higher, but the most massive mergers end up with the SF quenching; however, the core of the satellite moves inside the disc resembling the very latest stages of the merger. Since this has not yet occurred with the Sgr dwarf, this is beyond the interest of our work. In the right panel of Fig. 6, we show the ratio between the ISFR after and before the pericentric passage in interacting simulations only. This allows us to quantify how much the SF changed due to interaction.

It appears that only in a few models the SFR is increased by a factor of >3 , while in most of the cases, we detect an increase smaller than 2.

3.5 Metallicity variations caused by the interactions

A number of recent works focus on the effects of mergers in the metallicity distribution in simulated galaxies (Montuori et al. 2010;

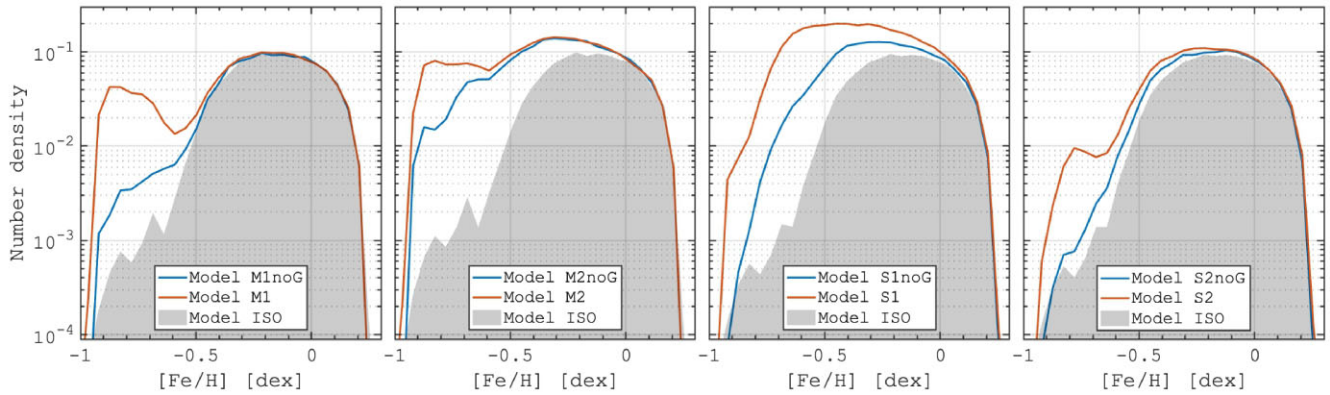


Figure 7. MDFs of stars formed inside the host galaxy. The grey area is the same across the panels and corresponds to the isolated galaxy simulation. Each panel shows a pair of simulations with the same orbit of the satellite galaxy where the MDFs are normalized by the total mass of stars formed in isolated simulation. The blue and red solid lines correspond to the model with a gasless satellite and a gas-rich satellite, respectively.

Rupke, Kewley & Barnes 2010; Torrey et al. 2012; Bustamante et al. 2018; Sparre et al. 2022; Khoperskov et al. 2023b). These works clearly show the ISM metallicity dilution effect in the central regions of the galaxy due to metal-poor gas being tidally funnelled into the centre during mergers. In agreement with the theoretical works, Bustamante et al. (2020) investigated a large sample of interacting galaxies from the Sloan Digital Sky Survey Data Release 7 and found an increasing gas-phase metallicity dilution and enhanced SF activity with decreasing separation between galaxies (see also e.g. Grønnow, Finlator & Christensen 2015).

These works study the major mergers of massive galaxies, which were completed on a short time-scale. However, the Sgr–MW interaction is less violent so far. In this section, we discuss the behaviour of the metallicity distribution in our simulations and some significant features caused by the perturbations from the satellites and corresponding gas infall on to the host galaxy. The particular details of the metallicity behaviour are dependent on the adopted initial metallicity; thus, we discuss only some general metallicity trends without giving any quantitative predictions regarding the metallicity distribution function (MDF) features caused by the Sgr dwarf galaxy in the MW.

First, in Fig. 7, we show the metallicity distributions for the stars formed inside the host galaxy. Each panel shows the MDFs from a pair of simulations with the same satellite orbit with gasless (blue) and gas-rich (red) satellite, which are compared to the MDF of the isolated host model (grey area). A striking feature of all our interacting simulations is the presence of a certain fraction of relatively low $[\text{Fe}/\text{H}]$ stars. In gasless satellite simulations (blue lines), the excess of low- $[\text{Fe}/\text{H}]$ stars results from the enhanced SF in the outer disc (see Fig. 4) where the ISM metallicity is low because of the imposed negative gradient in the ISM of the host (see Section 2.1 for details). We see that the only perturbation of the outer disc naturally leads to the formation of a non-negligible amount of stars with relatively low metallicity inherited from the ISM located in the outer disc.

The impact of the gas infall from satellites is clearly seen once we compare a pair of models in each panel of Fig. 7. First, the total mass of the low- $[\text{Fe}/\text{H}]$ stars is larger in gas-rich satellite simulations (red lines) than in gasless satellite simulations (blue lines), thus suggesting that some of the stars were formed *in situ* but in gas that was either directly accreted from satellites and/or mixed with the pre-existing gas of the host. Also, in most of the gas-rich satellite models, we see a second peak of the MDFs, which is not observed in the gasless

simulations. This further emphasizes the degree to which the gas from the satellite pollutes the host ISM and dilutes the metallicity of newly forming stars of the host, which is in agreement with Ruiz-Lara et al. (2016).

To highlight the effect of the metallicity dilution, we show the age–metallicity relation for the stars formed inside the host galaxies in Fig. 8. The ages of stars are indicative of their formation times in a manner where the youngest stars originate towards the end of the simulation, and the highest age corresponds to the simulation’s duration. The density distributions depict the MDF evolution as a function of time. The evolution of the mean metallicity in a particular model (white lines) is compared to the one in the isolated simulation (magenta lines). The effect of the metallicity dilution is inevitably linked to the close (<20 kpc) pericentric passages, where the mean metallicity decreases after the close approaches of the satellites. The dilution is more prominent in gas-rich satellite simulations because of the low- $[\text{Fe}/\text{H}]$ gas accretion on to the host galaxy. Note, however, that similar to the SFR behaviour (see Figs 2 and 3), the mean metallicity steadily decreases after the first close passage and does not show a quick recovery to its previous level. Hence, our simulations are in agreement with some previous studies (see e.g. Montuori et al. 2010, who showed that fly-bys of galaxies cause some dilution of the ISM metallicity). Moreover, some recent studies of the MW chemical compositions suggest a similar effect potentially associated with the Sgr and Gaia-Sausage-Enceladus (GSE) accretion events (Ciucă et al. 2023; Queiroz et al. 2023; Ratcliffe et al. 2023).

4 DISCUSSION

Using a set of models that are qualitatively similar to the ones we expect for the Sgr–MW interactions, we now discuss the implication of our models in the context of the MW evolution.

By using a colour-magnitude diagram (CMD) fitting technique, Ruiz-Lara et al. (2020) found an excess of stellar populations in several age bins, which were interpreted as bursts of the SF, ≈ 1 , 2, and 6 Gyr ago [note that Cignoni et al. (2006) and Sysoliatina & Just (2021) also found recent peaks of the SF in the SNd data]. Although the age distribution of stars in a local SNd-like region may not perfectly match the SFH of the entire galaxy in part because of stellar radial migration (Attard et al., in preparation), it was suggested that the bursts of the SF are real and correlate with the pericentric passages of the Sgr dwarf galaxy. Most of the dynamical models of

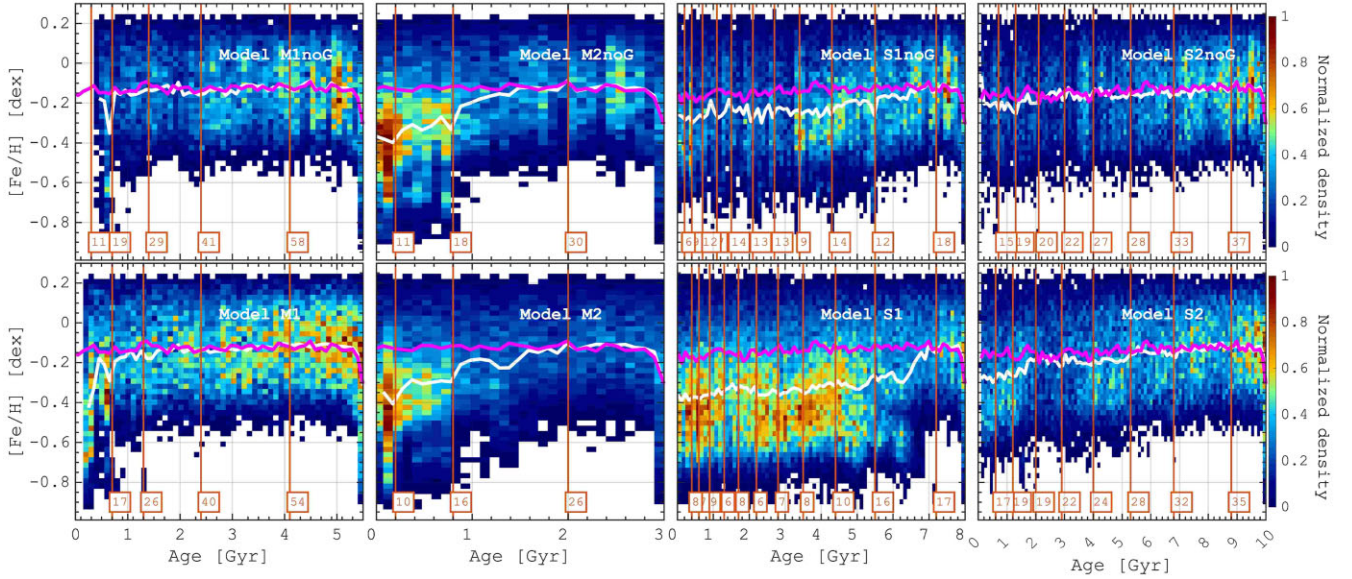


Figure 8. Age–metallicity relation of stars formed inside the host galaxy. The density maps are normalized by the maximum value in each panel. The red vertical lines correspond to the moments of pericentric passages of satellites, where the distance is marked in corresponding red boxes. The solid white and magenta lines show the evolution of the mean metallicity in a given model and in the isolated simulation, respectively.

the Sgr orbit suggest a couple of recent passages (≈ 1 and ≈ 2 Gyr ago) with pericentric distances of ≈ 10 – 20 kpc (e.g. Law & Majewski 2010; Łokas et al. 2010; Vasiliev & Belokurov 2020; Bennett et al. 2022), and since the present-day core of the Sgr galaxy does not contain gas (Tepper-García & Bland-Hawthorn 2018), these two conditions met in our models (see Fig. 2). Therefore, we confirm that the most recent passages of the Sgr dwarf galaxy indeed can have a significant impact on the SFH of the MW, similar to the one proposed by Ruiz-Lara et al. (2020). Note, however, that our models suggest that, in this case, the SF should be enhanced more in the outer disc (> 10 kpc, see Fig. 4), whose magnitude, however, should depend on the previous passages of the Sgr.

The moments of previous passages (> 3 Gyr ago) of the Sgr are less certain because of the initial mass and the mass-loss of the Sgr adopted in a given model. For instance, in the low-mass satellite simulations ($< 2 \times 10^{10} M_{\odot}$; e.g. Johnston, Hernquist & Bolte 1996; Peñarrubia et al. 2010; Hunt et al. 2021), we expect many pericentric passages (nearly for each Gyr back in time), which apparently were not detected in the SFH (2–5 Gyr ago) of the MW by Ruiz-Lara et al. (2020).

However, a very large mass of the Sgr progenitor (> 4 – $6 \times 10^{10} M_{\odot}$) at its first infall has been proposed in a number of different studies (see e.g. Jiang & Binney 2000; Gibbons et al. 2017; Read & Erkal 2019; Dillamore et al. 2022). The models that reproduce the best the correlation between the SF burst and pericentric passages of the Sgr are presented in Laporte et al. (2018b), where we focus on the first encounter. According to their models (L1, L2, H1, and H2), the Sgr’s infall t_{infall} should have happened 4–6 Gyr ago. Model L1 ($t_{\text{infall}} \approx 5.5$ Gyr ago) was already ruled out due to its inability to reproduce the outer structure of the MW (Laporte et al. 2018b). Models L2 and H2 show $t_{\text{infall}} \approx 4$ Gyr ago, which is by ≈ 1.5 Gyr off from the first and the most significant SF burst (≈ 6 Gyr) found by Ruiz-Lara et al. (2020). At the same time, the remaining model H1 ($t_{\text{infall}} \approx 5$ Gyr ago) marginally reproduces the Monoceros Ring (Laporte et al. 2018b).

Nevertheless, one could imagine that some models with parameters similar to H1/H2 and L2 from Laporte et al. (2018b) can simultaneously reproduce the outer MW disc features and predict the first pericentric passage exactly at the time expected from the MW SFH (≈ 6 Gyr ago). In this case, the first pericentre should be in the range of 30–40 kpc from the MW centre (see fig. 2 in Laporte et al. 2018b), otherwise, the dynamical friction would have already dragged a still quite massive Sgr to the MW centre because of a rather moderate mass-loss during pericentric passages (Tollet et al. 2017). At the first infall, the Sgr should be still relatively gas rich, which is supported by the SFH of the galaxy (Siegel et al. 2007; de Boer et al. 2015; Hasselquist et al. 2021). In this case, however, our models do not predict a coherent burst of SF (see Fig. 6). Therefore, in order to simultaneously account for a massive Sgr precursor at the first infall, its close first passage (< 20 kpc), and to avoid its fast subsequent coalescence with the MW, we require a substantial mass-loss during the first encounter (see e.g. Johnston, Spergel & Hernquist 1995), which is possibly even more significant than the one suggested by Bland-Hawthorn & Tepper-García (2021).

5 CONCLUSIONS

In this work, we have conducted a series of hydrodynamical simulations of interactions of the MW-type galaxies with massive satellites on quasi-polar orbits. We studied the purely dynamical impact of gasless satellites and a more complex evolution in the case of gas-rich satellites. The aim of our models is to address whether pericentric passages of satellites cause short-time-scale bursts of SF in the host galaxies. Although we found a substantial increase in the SFR in the host compared to isolated galaxy simulation, the details of the SFHs are highly dependent on the orbit and amount of gas in the satellite galaxies. Our main conclusions are summarized below.

- (i) Perturbations caused by the close passages of a massive satellite result in enhanced SF inside the MW-type discs. Prominent and short-term bursts of SF are the results of very close (< 20 kpc) pericentric

passages of massive ($2\text{--}6 \times 10^{10} M_{\odot}$) satellites, which do not contain gas (see Figs 2 and 6). For a given pericentric distance, the effect on SF is stronger in the case of a more massive satellite.

(ii) Interactions with gas-rich satellites result in even higher SFR enhancement; however, in this case, we do not detect prominent SF bursts unless the satellite passes through the disc of the host at the latest stages of coalescence. The reason for such behaviour is the steady accretion of gas from the satellite, which smoothens the overall SFR evolution in the host (see Fig. 3).

(iii) Independent of the gas content of the satellite, the SFR is mostly enhanced in the outer disc regions of the host after the first close (<20 kpc) pericentric passage. In particular, soon after the close pericentric passage, the SF is enhanced in the outer disc (>10 kpc), and then the SF propagates towards the centre of the host over the course of several Gyr. Therefore, we do not see an imminent impact on the inner SF of the host galaxy in case of close passages of gas-rich satellites (see Fig. 4).

(iv) The increase of the SF in the outer disc of the host results in the excess of stars with lower [Fe/H], which is being inherited from the ISM at the outskirts (see Figs 7 and 8). The effect of stellar metallicity dilution is seen in both gasless and gas-rich satellite simulations, where it is more prominent in gas-rich satellite simulations due to low-[Fe/H] gas accretion on to the host galaxy.

(v) Our simulations are in favour of the causality between the latest passages of the Sgr galaxy and the bursts of the SF in the SND at ≈ 1 and ≈ 2 Gyr (Ruiz-Lara et al. 2020; Sysoliatina & Just 2021). However, according to our model, a potential burst at ≈ 6 Gyr (Ruiz-Lara et al. 2020) requires a very close passage (<20 kpc from the MW centre) of a massive ($>2 \times 10^{10} M_{\odot}$) Sgr precursor with a very substantial mass-loss allowing to prevent a rapid coalescence with the MW until the present.

ACKNOWLEDGEMENTS

We sincerely thank the referee for a thoughtful review of our paper. BA thanks the AIP for the access to the institute's infrastructure during his remote internship. This work has made use of the computational resources available at the AIP, as well as those obtained through the DARI grant A1020410154 (PI: P. Di Matteo). SK thanks participants of weekly chemodynamics meetings at the AIP for their useful suggestions regarding the results of this work.

DATA AVAILABILITY

The data supporting this article will be shared upon reasonable request sent to the corresponding authors.

REFERENCES

Antoja T. et al., 2018, *Nature*, 561, 360
 Bailin J., 2003, *ApJ*, 583, L79
 Barnes J. E., Hernquist L. E., 1991, *ApJ*, 370, L65
 Bennett M., Bovy J., 2021, *MNRAS*, 503, 376
 Bennett M., Bovy J., Hunt J. A. S., 2022, *ApJ*, 927, 131
 Bland-Hawthorn J., Gerhard O., 2016, *ARA&A*, 54, 529
 Bland-Hawthorn J., Tepper-García T., 2021, *MNRAS*, 504, 3168
 Bland-Hawthorn J. et al., 2019, *MNRAS*, 486, 1167
 Bustamante S., Sparre M., Springel V., Grand R. J. J., 2018, *MNRAS*, 479, 3381
 Bustamante S., Ellison S. L., Patton D. R., Sparre M., 2020, *MNRAS*, 494, 3469
 Carr C., Johnston K. V., Laporte C. F. P., Ness M. K., 2022, *MNRAS*, 516, 5067

Cignoni M., Degl'Innocenti S., Prada Moroni P. G., Shore S. N., 2006, *A&A*, 459, 783
 Ciucă I. et al., 2023, *MNRAS*
 Cox T. J., Jonsson P., Somerville R. S., Primack J. R., Dekel A., 2008, *MNRAS*, 384, 386
 D'Onghia E., Madau P., Vera-Ciro C., Quillen A., Hernquist L., 2016, *ApJ*, 823, 4
 D'Souza R., Bell E. F., 2022, *MNRAS*, 512, 739
 Darling K., Widrow L. M., 2019, *MNRAS*, 484, 1050
 de Boer T. J. L., Belokurov V., Koposov S., 2015, *MNRAS*, 451, 3489
 de la Vega A., Quillen A. C., Carlin J. L., Chakrabarti S., D'Onghia E., 2015, *MNRAS*, 454, 933
 Di Cintio A., Mostoghiu R., Knebe A., Navarro J. F., 2021, *MNRAS*, 506, 531
 Di Matteo P., Combes F., Melchior A. L., Semelin B., 2007, *A&A*, 468, 61
 Di Matteo P., Bournaud F., Martig M., Combes F., Melchior A. L., Semelin B., 2008, *A&A*, 492, 31
 Dierickx M. I. P., Loeb A., 2017, *ApJ*, 836, 92
 Dillamore A. M., Belokurov V., Evans N. W., Price-Whelan A. M., 2022, *MNRAS*, 516, 1685
 Dobbs C. L., Theis C., Pringle J. E., Bate M. R., 2010, *MNRAS*, 403, 625
 Drimmel R., Spergel D. N., 2001, *ApJ*, 556, 181
 Dwek E. et al., 1995, *ApJ*, 445, 716
 Gaia Collaboration, 2018, *A&A*, 616, A10
 Gibbons S. L. J., Belokurov V., Evans N. W., 2017, *MNRAS*, 464, 794
 Gómez F. A., Minchev I., O'Shea B. W., Beers T. C., Bullock J. S., Purcell C. W., 2013, *MNRAS*, 429, 159
 Gómez F. A., Besla G., Carpintero D. D., Villalobos Á., O'Shea B. W., Bell E. F., 2015, *ApJ*, 802, 128
 Grønnow A. E., Finlator K., Christensen L., 2015, *MNRAS*, 451, 4005
 Hasselquist S. et al., 2021, *ApJ*, 923, 172
 Hopkins P. F., 2015, *MNRAS*, 450, 53
 Hopkins P. F., 2017, preprint (arXiv:1712.01294)
 Hopkins P. F., Cox T. J., Hernquist L., Narayanan D., Hayward C. C., Murray N., 2013a, *MNRAS*, 430, 1901
 Hopkins P. F., Narayanan D., Murray N., 2013b, *MNRAS*, 432, 2647
 Hunt J. A. S., Stelea I. A., Johnston K. V., Gandhi S. S., Laporte C. F. P., Bédorf J., 2021, *MNRAS*, 508, 1459
 Ibata R. A., Razoumov A. O., 1998, *A&A*, 336, 130
 Ibata R. A., Gilmore G., Irwin M. J., 1994, *Nature*, 370, 194
 Ibata R. A., Gilmore G., Irwin M. J., 1995, *MNRAS*, 277, 781
 Jiang I.-G., Binney J., 2000, *MNRAS*, 314, 468
 Jog C. J., Solomon P. M., 1992, *ApJ*, 387, 152
 Johnston K. V., Spergel D. N., Hernquist L., 1995, *ApJ*, 451, 598
 Johnston K. V., Hernquist L., Bolte M., 1996, *ApJ*, 465, 278
 Kerr F. J., 1957, *AJ*, 62, 93
 Khoperskov S., Di Matteo P., Gerhard O., Katz D., Haywood M., Combes F., Berczik P., Gomez A., 2019, *A&A*, 622, L6
 Khoperskov S. et al., 2023a, *A&A*, 677, A89
 Khoperskov S. et al., 2023b, *A&A*, 677, A91
 Laporte C. F. P., Gómez F. A., Besla G., Johnston K. V., Garavito-Camargo N., 2018a, *MNRAS*, 473, 1218
 Laporte C. F. P., Johnston K. V., Gómez F. A., Garavito-Camargo N., Besla G., 2018b, *MNRAS*, 481, 286
 Laporte C. F. P., Minchev I., Johnston K. V., Gómez F. A., 2019, *MNRAS*, 485, 3134
 Law D. R., Majewski S. R., 2010, *ApJ*, 714, 229
 Layden A. C., Sarajedini A., 2000, *AJ*, 119, 1760
 Łokas E. L., Kazantzidis S., Majewski S. R., Law D. R., Mayer L., Frinchaboy P. M., 2010, *ApJ*, 725, 1516
 Lu Y., Minchev I., Buck T., Khoperskov S., Steinmetz M., Libeskind N., Cescutti G., Freeman K. C., 2022, preprint (arXiv:2212.04515)
 Massana P. et al., 2022, *MNRAS*, 513, L40
 Michel-Dansac L., Abadi M. G., Navarro J. F., Steinmetz M., 2011, *MNRAS*, 414, L1
 Mihos J. C., Hernquist L., 1994, *ApJ*, 425, L13
 Miyamoto M., Nagai R., 1975, *PASJ*, 27, 533

- Montuori M., Di Matteo P., Lehnert M. D., Combes F., Semelin B., 2010, *A&A*, 518, A56
- Moreno J., Torrey P., Ellison S. L., Patton D. R., Bluck A. F. L., Bansal G., Hernquist L., 2015, *MNRAS*, 448, 1107
- Ness M., Lang D., 2016, *AJ*, 152, 14
- Pasetto S., Grebel E. K., Berczik P., Chiosi C., Spurzem R., 2011, *A&A*, 525, A99
- Peñarrubia J., Belokurov V., Evans N. W., Martínez-Delgado D., Gilmore G., Irwin M., Niederste-Ostholt M., Zucker D. B., 2010, *MNRAS*, 408, L26
- Pettitt A. R., Tasker E. J., Wadsley J. W., 2016, *MNRAS*, 458, 3990
- Pettitt A. R., Tasker E. J., Wadsley J. W., Keller B. W., Benincasa S. M., 2017, *MNRAS*, 468, 4189
- Plummer H. C., 1911, *MNRAS*, 71, 460
- Poggio E. et al., 2018, *MNRAS*, 481, L21
- Purcell C. W., Bullock J. S., Tollerud E. J., Rocha M., Chakrabarti S., 2011, *Nature*, 477, 301
- Queiroz A. B. A. et al., 2023, *A&A*, 673, A155
- Ratcliffe B. et al., 2023, *MNRAS*, 525, 2208
- Read J. I., Erkal D., 2019, *MNRAS*, 487, 5799
- Reid M. J. et al., 2009, *ApJ*, 700, 137
- Renaud F., Boily C. M., Naab T., Theis C., 2009, *ApJ*, 706, 67
- Renaud F., Bournaud F., Kraljic K., Duc P. A., 2014, *MNRAS*, 442, L33
- Renaud F., Agertz O., Read J. I., Ryde N., Andersson E. P., Bensby T., Rey M. P., Feuillet D. K., 2021, *MNRAS*, 503, 5846
- Renaud F., Segovia Otero Á., Agertz O., 2022, *MNRAS*, 516, 4922
- Ruiz-Lara T., Few C. G., Gibson B. K., Pérez I., Florido E., Minchev I., Sánchez-Blázquez P., 2016, *A&A*, 586, A112
- Ruiz-Lara T., Gallart C., Bernard E. J., Cassisi S., 2020, *Nat. Astron.*, 4, 965
- Ruiz-Lara T. et al., 2021, *MNRAS*, 501, 3962
- Rupke D. S. N., Kewley L. J., Barnes J. E., 2010, *ApJ*, 710, L156
- Rusakov V., Monelli M., Gallart C., Fritz T. K., Ruiz-Lara T., Bernard E. J., Cassisi S., 2021, *MNRAS*, 502, 642
- Schönrich R., Dehnen W., 2018, *MNRAS*, 478, 3809
- Siegel M. H. et al., 2007, *ApJ*, 667, L57
- Sohn S. T. et al., 2007, *ApJ*, 663, 960
- Sparre M., Springel V., 2016, *MNRAS*, 462, 2418
- Sparre M., Whittingham J., Damle M., Hani M. H., Richter P., Ellison S. L., Pfrommer C., Vogelsberger M., 2022, *MNRAS*, 509, 2720
- Springel V., Hernquist L., 2003, *MNRAS*, 339, 312
- Springel V., Di Matteo T., Hernquist L., 2005, *MNRAS*, 361, 776
- Sysoliatina K., Just A., 2021, *A&A*, 647, A39
- Taibi S., Battaglia G., Leaman R., Brooks A., Riggs C., Munshi F., Revaz Y., Jablonka P., 2022, *A&A*, 665, A92
- Tepper-García T., Bland-Hawthorn J., 2018, *MNRAS*, 478, 5263
- Tollet É., Cattaneo A., Mamon G. A., Moutard T., van den Bosch F. C., 2017, *MNRAS*, 471, 4170
- Torrey P., Cox T. J., Kewley L., Hernquist L., 2012, *ApJ*, 746, 108
- Vallée J. P., 2005, *AJ*, 130, 569
- Vasiliev E., 2019, *MNRAS*, 482, 1525
- Vasiliev E., Belokurov V., 2020, *MNRAS*, 497, 4162
- Vasiliev E., Belokurov V., Erkal D., 2021, *MNRAS*, 501, 2279
- Wegg C., Gerhard O., 2013, *MNRAS*, 435, 1874

This paper has been typeset from a $\text{\TeX}/\text{\LaTeX}$ file prepared by the author.